SUPPLEMENTARY INFORMATION

Metabolic drug survey highlights cancer cell dependencies and vulnerabilities

T. Pemovska, J. W. Bigenzahn, I. Srndic, A. Lercher, A. Bergthaler, A. César-Razquin, F. Kartnig, C. Kornauth, P. Valent, P. B. Staber, G. Superti-Furga.

Content of Supplementary Information:

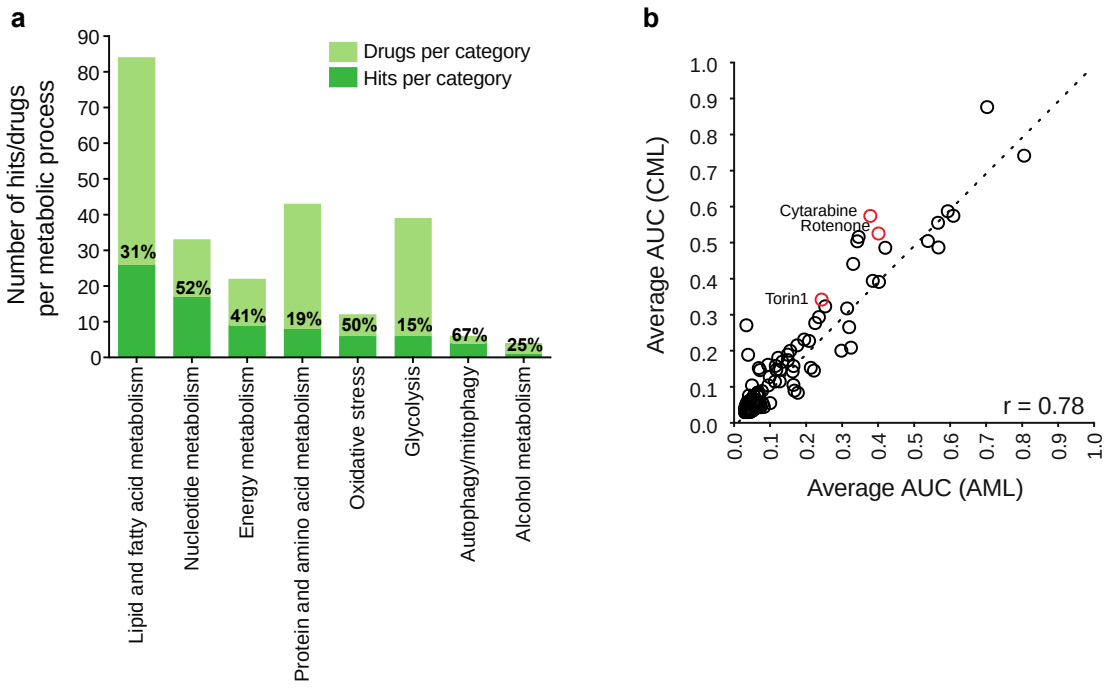

Supplementary Fig. 1| Distribution of metabolic inhibitors affecting cellular viability per metabolic pathway / process and identification of selectively acting compounds in disease-specific manner. a, Metabolic pathway coverage of compounds that had an effect on cell viability in the tested cell lines highlighting the percentage of hits in relation of all compounds in a given metabolic category. **b**, Correlation of the average metabolic drug sensitivity profile of AML and CML cell lines showing disease specific vulnerabilities.

a

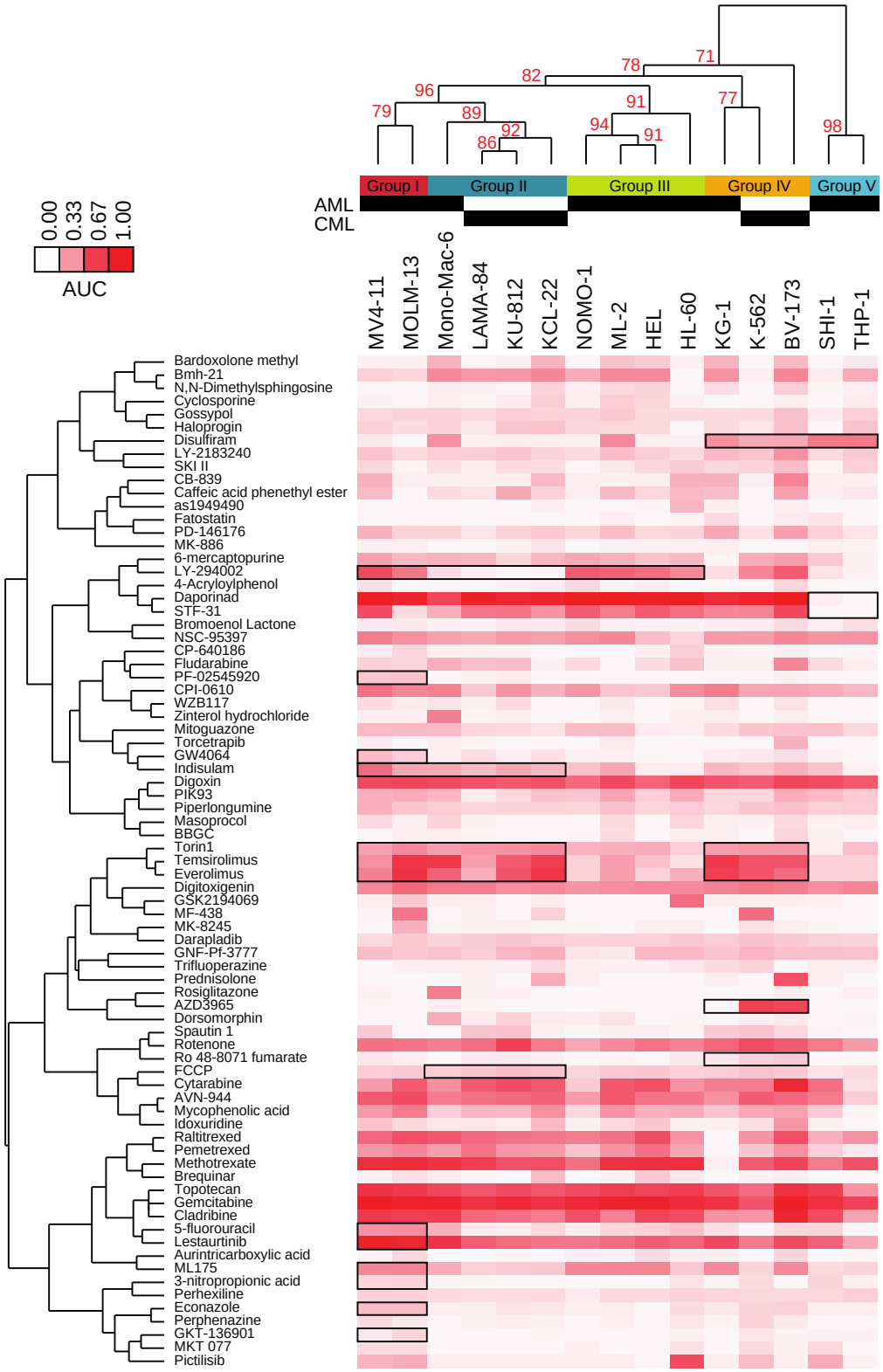
0.00
0.33
0.67
1.00
AUC
71
78
82
96
79
89
92
86
91
94
91
77
98
Group I
Group II
Group III
Group IV
Group V
AML
CML
MV4-11
MOLM-13
Mono-Mac-6
LAMA-84
KU-812
KCL-22
NOMO-1
ML-2
HEL
HL-60
KG-1
K-562
BV-173
SHI-1
THP-1
Bardoxolone methyl
Bmh-21
N,N-Dimethylsphingosine
Cyclosporine
Gossypol
Haloprogin
Disulfiram
LY-2183240
SKI II
CB-839
Caffeic acid phenethyl ester
as1949490
Fatostatin
PD-146176
MK-886
6-mercaptopurine
LY-294002
4-Acryloylphenol
Daporinad
STF-31
Bromoenol Lactone
NSC-95397
CP-640186
Fludarabine
PF-02545920
CPI-0610
WZB117
Zinterol hydrochloride
Mitoguazone
Torcetrapib
GW4064
Indisulam
Digoxin
PIK93
Piperlongumine
Masoprocol
BBGC
Torin1
Temsirolimus
Everolimus
Digitoxigenin
GSK2194069
MF-438
MK-8245
Darapladib
GNF-Pf-3777
Trifluoperazine
Prednisolone
Rosiglitazone
AZD3965
Dorsomorphin
Spautin 1
Rotenone
Ro 48-8071 fumarate
FCCP
Cytarabine
AVN-944
Mycophenolic acid
Idoxuridine
Raltitrexed
Pemetrexed
Methotrexate
Brequinar
Topotecan
Gemcitabine
Cladribine
5-fluorouracil
Lestaurtinib
Aurintricarboxylic acid
ML175
3-nitropropionic acid
Perhexiline
Econazole
Perphenazine
GKT-136901
MKT 077
Pictilisib

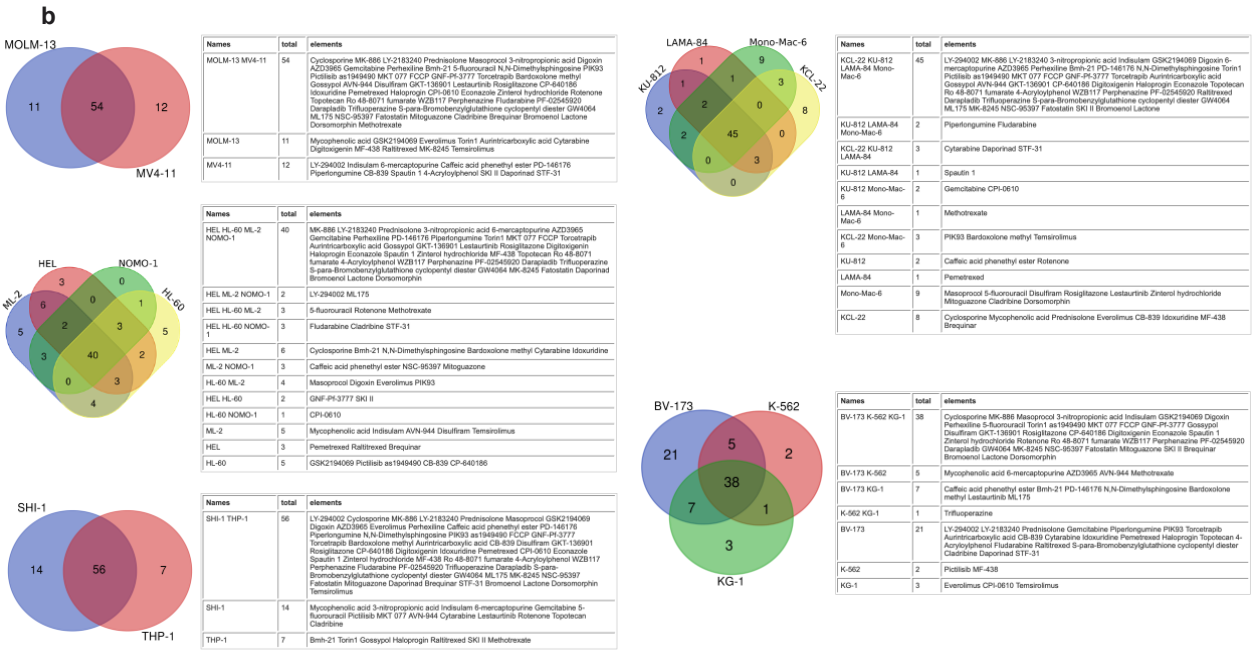

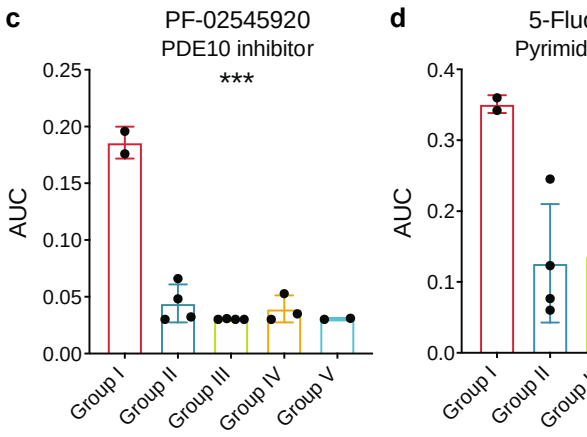

Supplementary Fig. 2| Metabolic drug sensitivity testing classifies myeloid leukemia cell lines in 5 functional groups. a, Unsupervised hierarchical clustering of the 77 viability affecting drugs is presented as a heatmap across 15 cell lines.

Clustering was performed using the complete linkage clustering method and Euclidian and Spearman distance measures of the AUC values of cell lines and drugs, respectively. The response profiles of several compounds and compounds classes display differential effects across the cell lines tested and are outlined with black boxes. The reproducibility of the clusters was evaluated by randomly resampling 10,000 bootstrap samples of the original dataset and calculating the frequency at which each cluster appears in the hierarchical clustering of the bootstrap replicates. The numbers in the dendrogram tree of the cell lines indicate the approximately unbiased (AU) empirical frequencies (0-100%) from the multiscale bootstrap resampling implemented in the Pvclust R-package. **b**, Venn diagrams depicting concordant and discordant drug responses within the functional taxonomic clusters defined in Fig. 2c. **c-h**, Bar graphs depicting the distribution of AUC values for selected compounds significantly contributing to the grouping of cell lines (Group I, n=2; Group II, n=4; Group III, n=4; Group IV, n=3; and Group V, n=2) shown in **Fig. 2** (an ordinary one-way ANOVA analysis; FDR of 10% was deemed significant; * *P*adj $\leq$ 0.1; ** *P*adj $\leq$ 0.05; *** *P*adj $\leq$ 0.01; ns not significant). Error bars indicate mean $\pm$ SD.

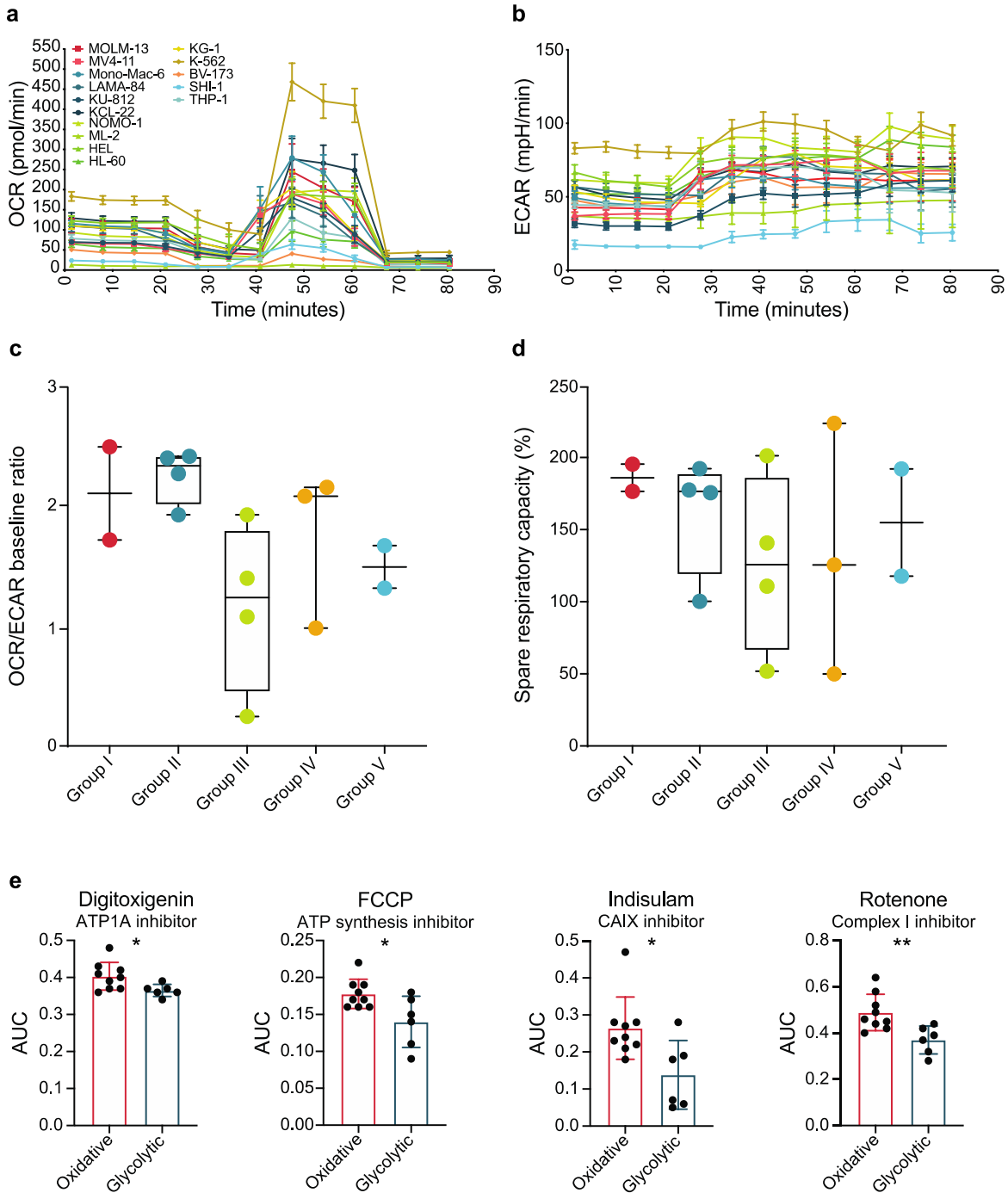

Supplementary Fig. 3| Metabolic phenotypes of the myeloid leukemia cell lines. **a**-**b**, Measurement of oxygen consumption rate (OCR) and extracellular acidification rate (ECAR) with the Seahorse analyzer XF96 at basal level and after consecutive injections of oligomycin (1μM), FCCP (1μM), and antimycin A (1μM) / rotenone (1μM) (n = 8 technical replicates; error bars mean ± SD). **c**-**d**, Box and whiskers (min to max) plot showing the basal bioenergetics state (the mean OCR at baseline (n = 8 technical

replicates) divided by the mean ECAR at baseline (n = 8 technical replicates) for each individual cell line (n=15) from the second baseline timepoint at approximately 8 minutes after assay start) and percentage spare respiratory capacity of the myeloid cell lines. The black line in the middle of the box depicts the median and the box extends from the 25th to 75th percentiles. **e**, Bar graph illustrating a significant difference in sensitivity to inhibitors targeting energy metabolism between more oxidative cell lines (ones falling in Group I, II and IV; n=9) and the more glycolytic cell lines (ones in Group III and V; n=6). Data is presented as mean ± SD; Unpaired two-tailed T-test; * $P < 0.05$, ** $P < 0.01$ (digitoxigenin $P = 0.0358$; FCCP $P = 0.0182$; indisulam $P = 0.0272$; rotenone $P = 0.0081$).

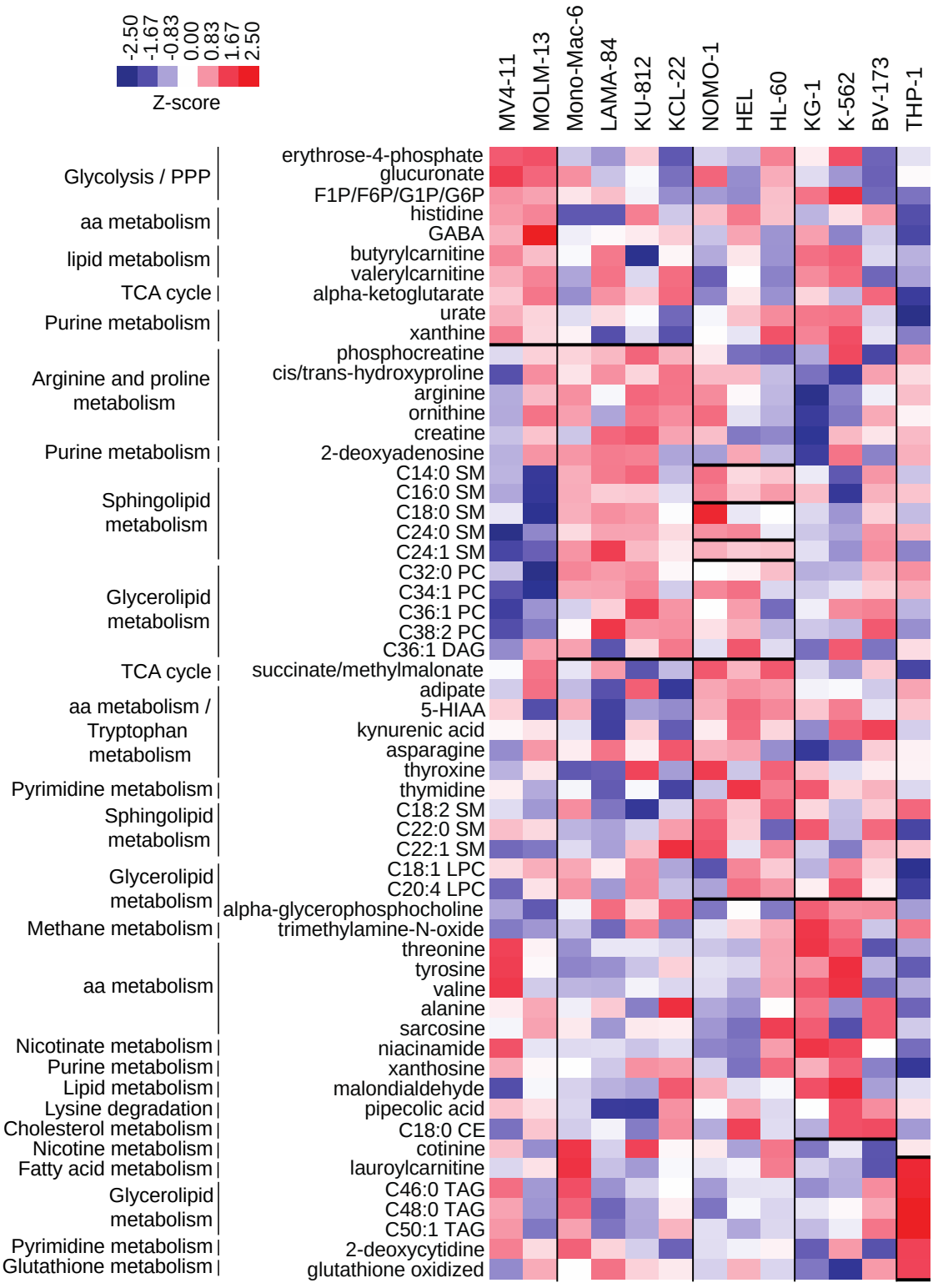

Supplementary Fig. 4| Analysis of publicly available targeted metabolomics data from the CCLE Resource[1]. The levels of 57 metabolites, represented as Z-scores and visualized with a heatmap, were significantly different between at least two of the drug sensitivity pre-defined groups with a two-way ANOVA analysis (FDR of 10% was

deemed significant). For analysis the clean imputed Log2 transformed values provided in the original publication were used.

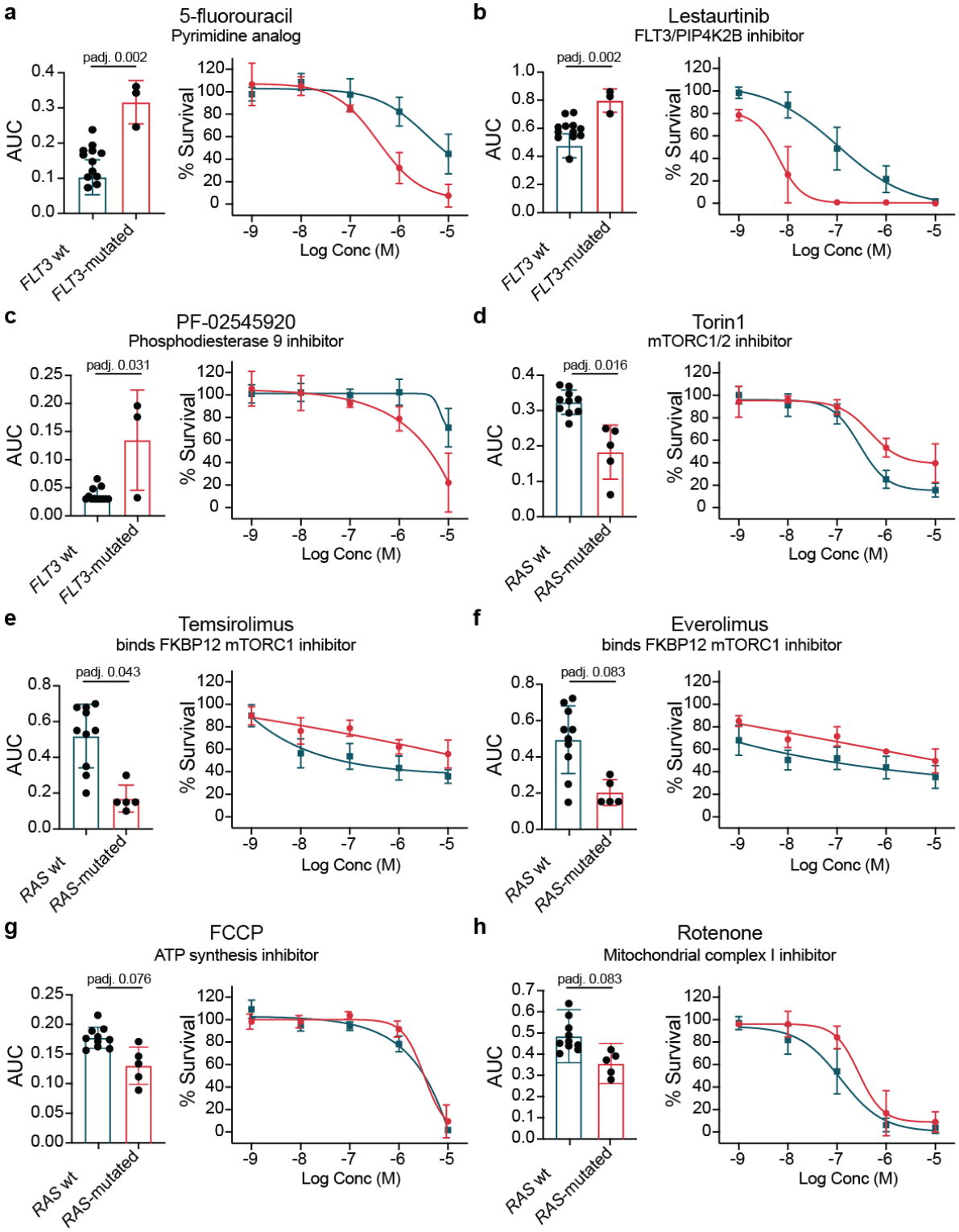
a
5-fluorouracil
Pyrimidine analog
padj. 0.002
AUC
FLT3 wt
FLT3-mutated
% Survival
Log Conc (M)
b
Lestaurtinib
FLT3/PIP4K2B inhibitor
padj. 0.002
c
PF-02545920
Phosphodiesterase 9 inhibitor
padj. 0.031
d
Torin1
mTORC1/2 inhibitor
padj. 0.016
RAS wt
RAS-mutated
e
Temsirolimus
binds FKBP12 mTORC1 inhibitor
padj. 0.043
f
Everolimus
binds FKBP12 mTORC1 inhibitor
padj. 0.083
g
FCCP
ATP synthesis inhibitor
padj. 0.076
h
Rotenone
Mitochondrial complex I inhibitor
padj. 0.083

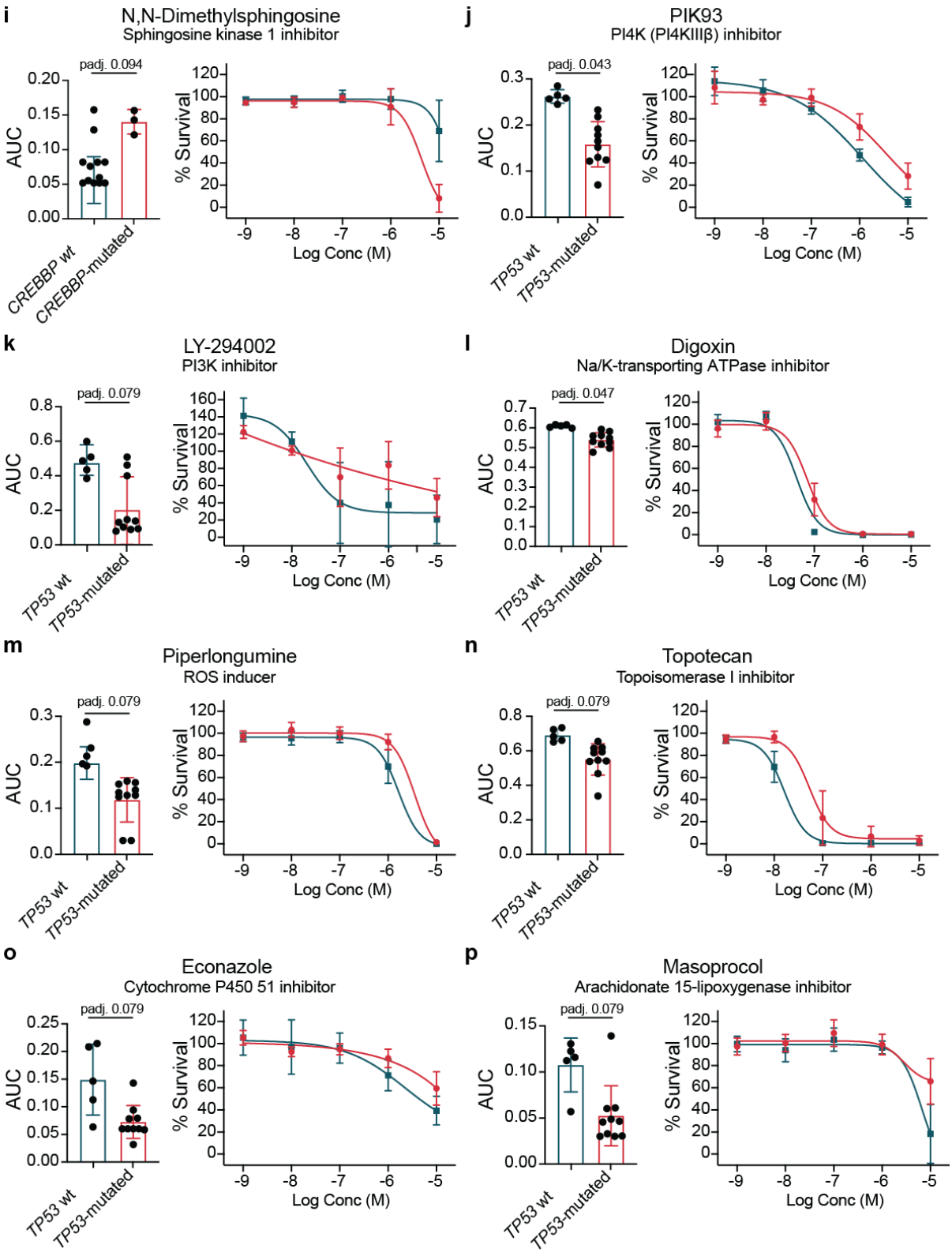

Supplementary Fig. 5| Significant genotype to phenotype associations. a-p, Box-plots and mean dose response curves depicting sensitivity of several metabolic modifiers that have significantly higher or lower sensitivity in *FLT3-ITD* (**a-c**), *RAS* (**d-**

h), *CREBBP* (**i**), and *TP53* (**j**-**p**) mutant versus wild-type cell lines as depicted in **Fig. 3a**. Error bars signify mean ± SD and the difference in response was assessed with a two-tailed unpaired *T*-test after multiple testing correction (FDR of 10% was deemed significant; * *P*adj ≤ 0.1; ** *P*adj < 0.05; *** *P*adj < 0.01).

HL-60

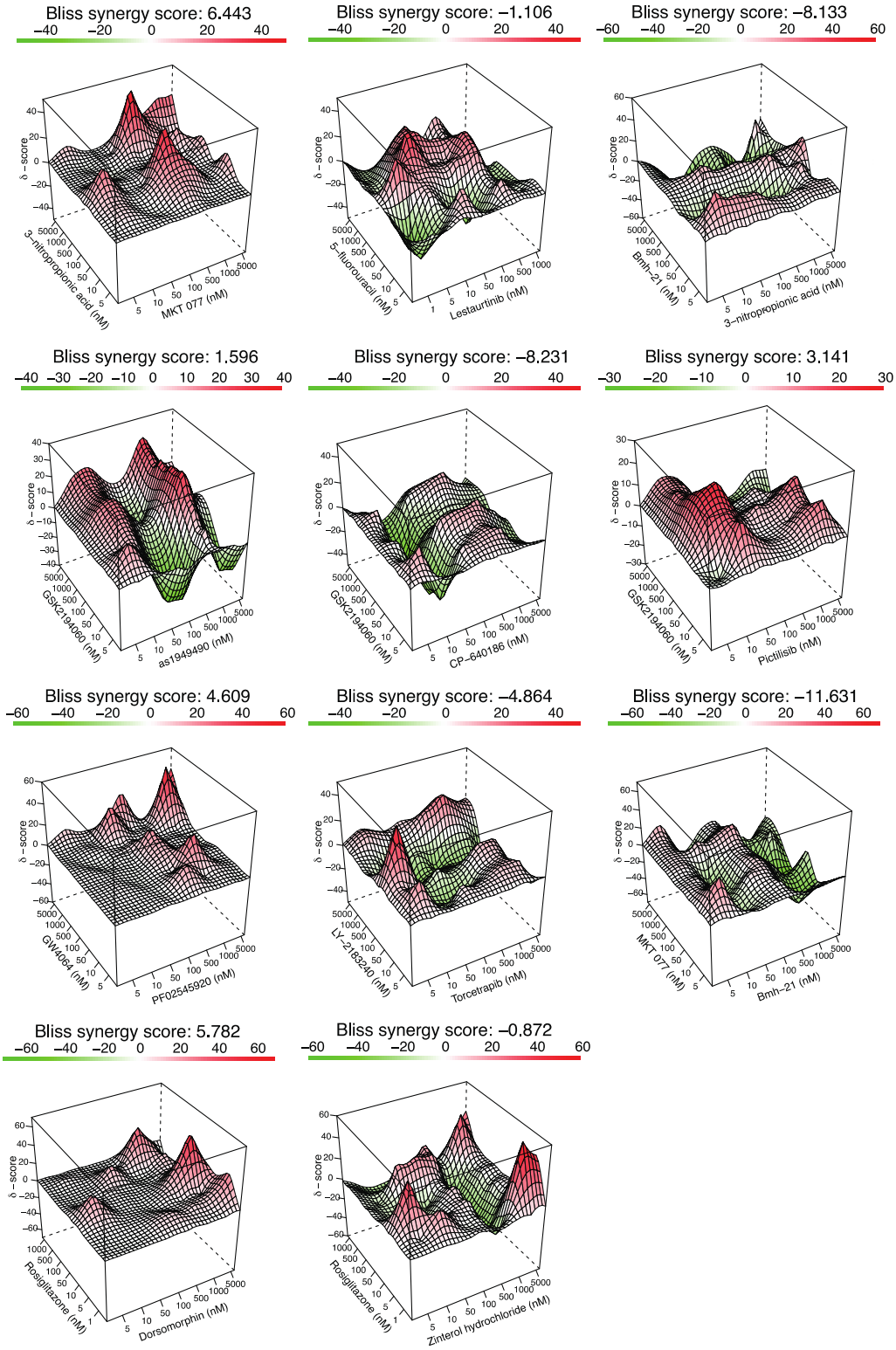
Bliss synergy score: 6.443
3−nitropropionic acid (nM)
MKT 077 (nM)
Bliss synergy score: −1.106
5−fluorouracil (nM)
Lestaurtinib (nM)
Bliss synergy score: −8.133
Bmh−21 (nM)
3−nitropropionic acid (nM)
Bliss synergy score: 1.596
GSK2194060 (nM)
as1949490 (nM)
Bliss synergy score: −8.231
GSK2194060 (nM)
CP−640186 (nM)
Bliss synergy score: 3.141
GSK2194060 (nM)
Pictilisib (nM)
Bliss synergy score: 4.609
GW4064 (nM)
PF02545920 (nM)
Bliss synergy score: −4.864
LY−2183240 (nM)
Torcetrapib (nM)
Bliss synergy score: −11.631
MKT 077 (nM)
Bmh−21 (nM)
Bliss synergy score: 5.782
Rosiglitazone (nM)
Dorsomorphin (nM)
Bliss synergy score: −0.872
Rosiglitazone (nM)
Zinterol hydrochloride (nM)

Mono-Mac-6

Bliss synergy score: −1.583

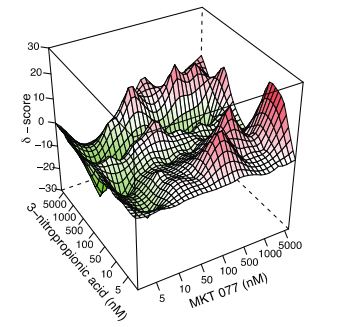

Bliss synergy score: −3.075

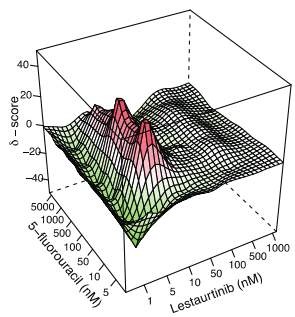

Bliss synergy score: 2.129

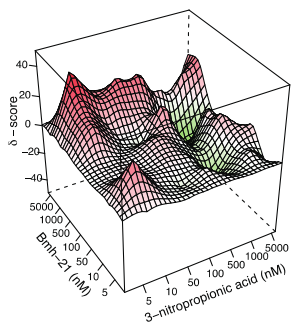

Bliss synergy score: 3.316

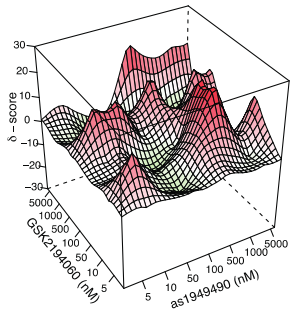

Bliss synergy score: −0.038

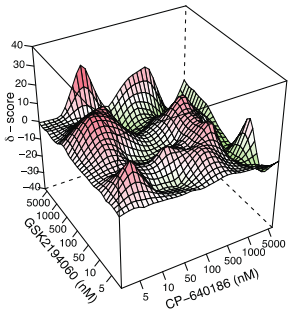

Bliss synergy score: −2.966

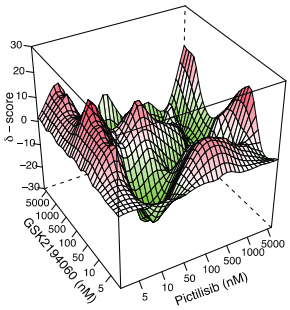

Bliss synergy score: −5.222

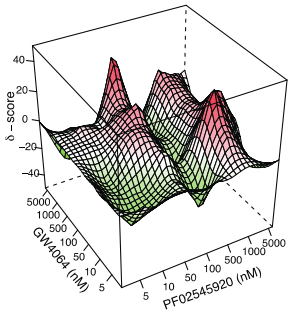

Bliss synergy score: −2.178

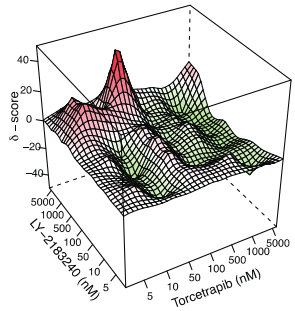

Bliss synergy score: 3.269

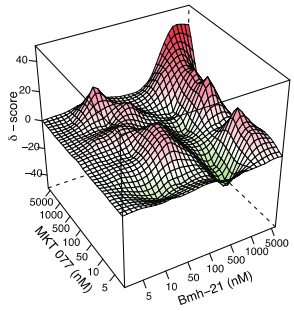

Bliss synergy score: −4.162

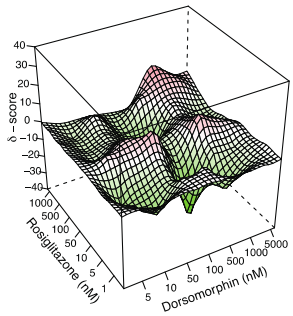

Bliss synergy score: 7.966

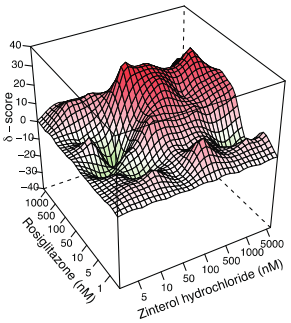

BV-173

Bliss synergy score: 1.033

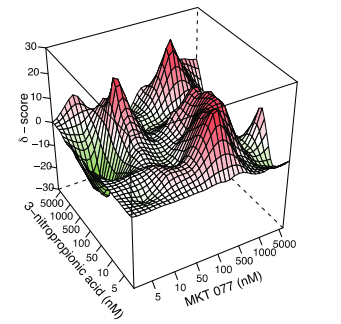

Bliss synergy score: –4.795

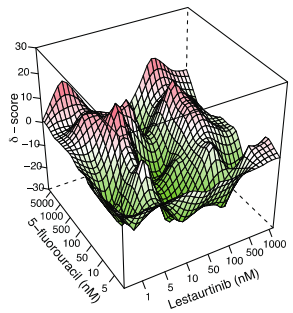

Bliss synergy score: 1.284

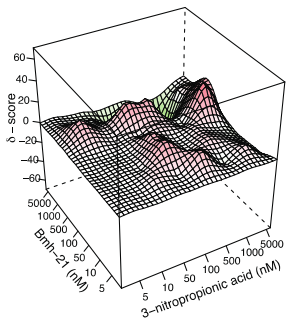

Bliss synergy score: 4.085

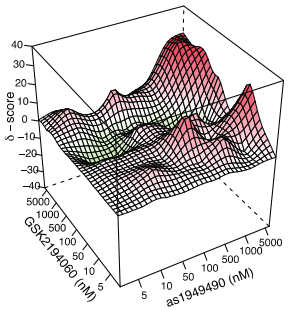

Bliss synergy score: –0.61

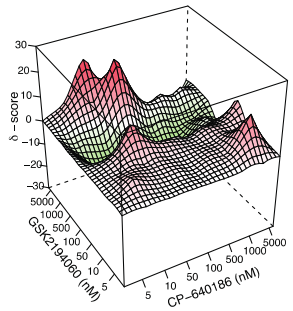

Bliss synergy score: 1.962

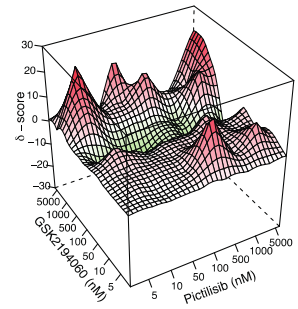

Bliss synergy score: 0.598

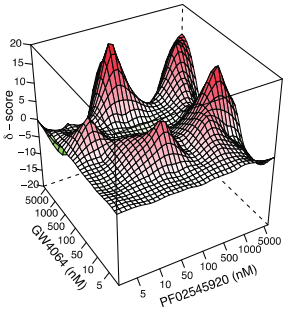

Bliss synergy score: 3.713

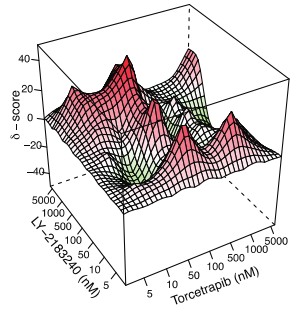

Bliss synergy score: –5.216

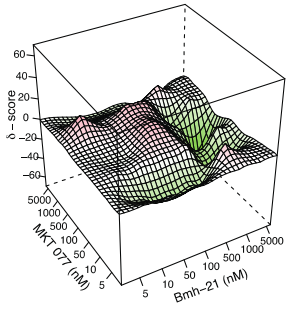

Bliss synergy score: –1.574

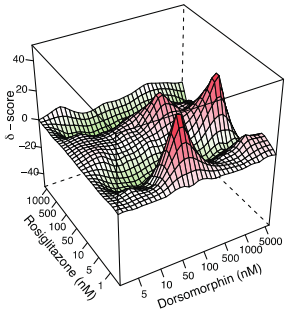

Bliss synergy score: –2.965

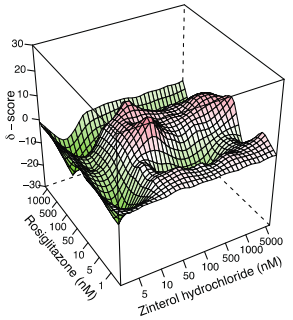

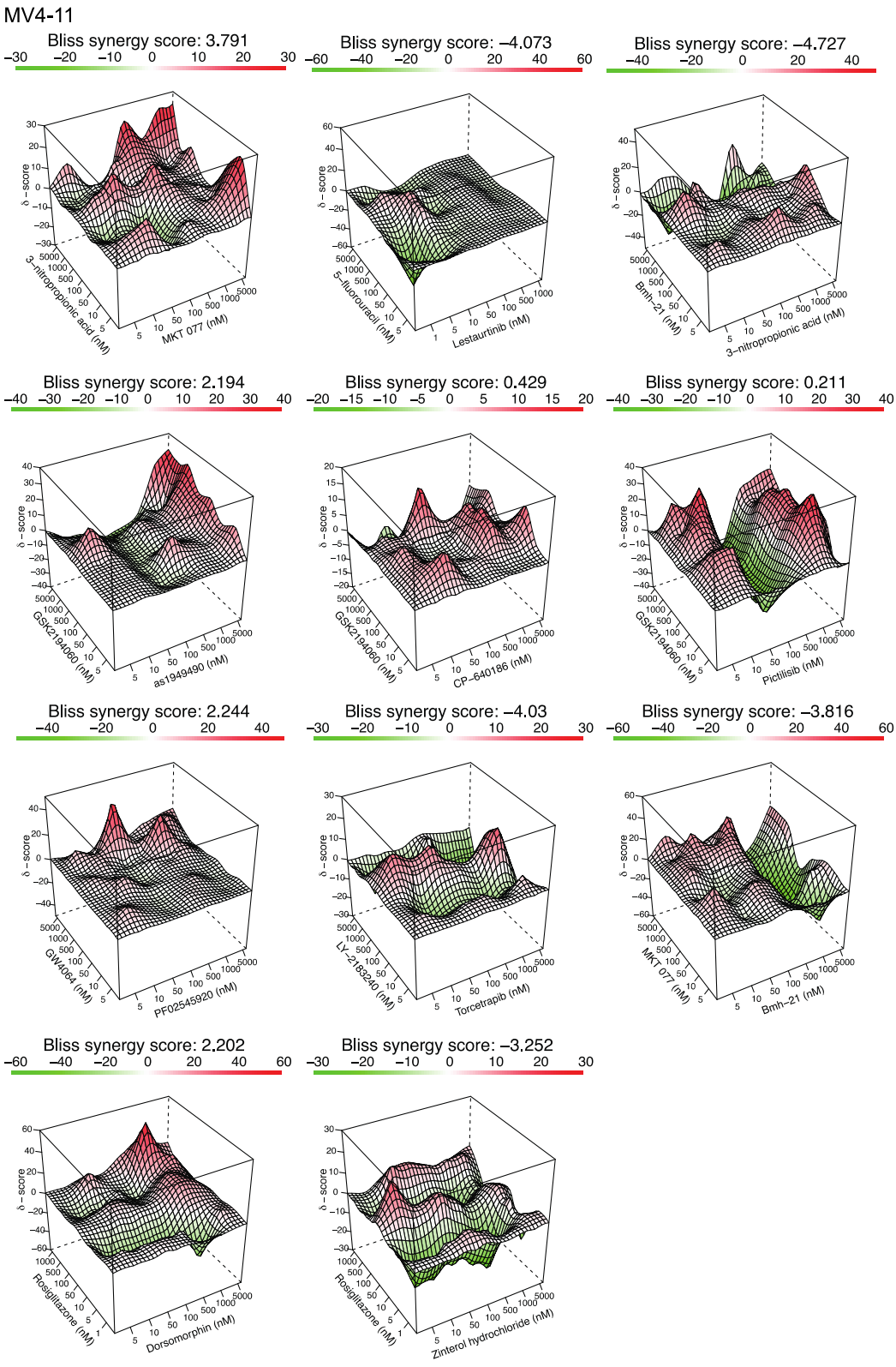

Supplementary Fig. 6| 3D drug synergy visualizations for 11 different drug-drug interactions in HL-60, Mono-Mac-6, BV-173, and MV4-11 cells. Data was generated in 8x8 drug synergy matrices and analyzed using the SynergyFinder tool

using the Bliss independence model with % survival values at each tested concertation relative to DMSO (negative control) and 10µM bortezomib (positive control). The synergy score for a drug combination is averaged over all the dose combination measurments. The 2D and 3D synergy maps highlight synergistic and antagonistic dose regions in red and green, respectively.

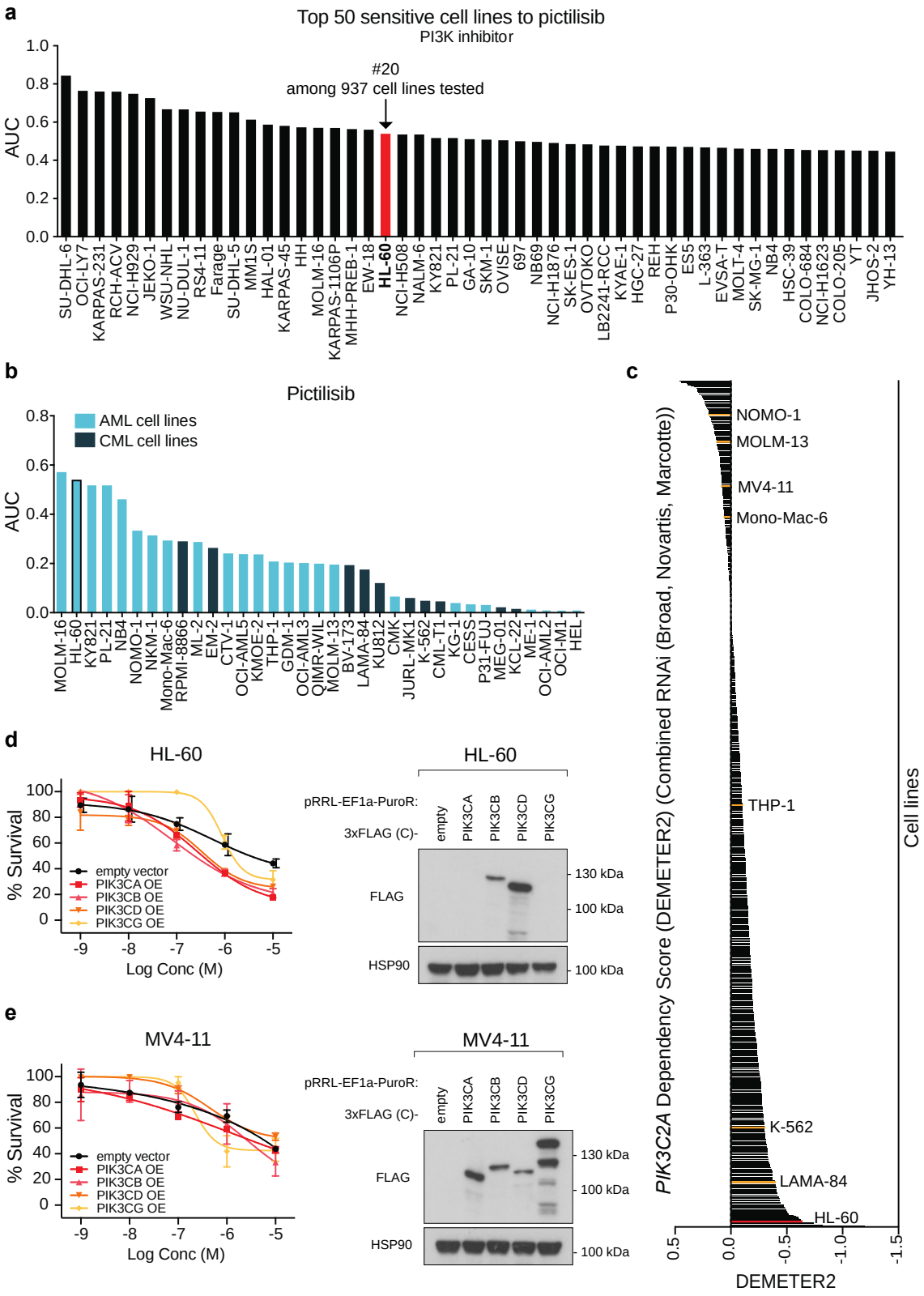
a
Top 50 sensitive cell lines to pictilisib
PI3K inhibitor
#20
among 937 cell lines tested
AUC
SU-DHL-6 OCI-LY7 KARPAS-231 RCH-ACV NCI-H929 JEKO-1 WSU-NHL NU-DUL-1 RS4-11 Farage SU-DHL-5 MM1S HAL-01 KARPAS-45 HH MOLM-16 KARPAS-1106P MHH-PREB-1 EW-18 HL-60 NCI-H508 NALM-6 KY821 PL-21 GA-10 SKM-1 OVISE 697 NB69 NCI-H1876 SK-ES-1 OVTOKO LB2241-RCC KYAE-1 HGC-27 REH P30-OHK ES5 L-363 EVSA-T MOLT-4 SK-MG-1 NB4 HSC-39 COLO-684 NCI-H1623 COLO-205 YT JHOS-2 YH-13
b
Pictilisib
AML cell lines
CML cell lines
AUC
MOLM-16 HL-60 KY821 PL-21 NB4 NOMO-1 NKM-1 Mono-Mac-6 RPMI-8866 ML-2 EM-2 CTV-1 OCI-AML5 KMOE-2 THP-1 GDM-1 OCI-AML3 QIMR-WIL MOLM-13 BV-173 LAMA-84 KU812 CMK JURL-MK1 K-562 CML-T1 KG-1 CESS P31-FUJ MEG-01 KCL-22 ME-1 OCI-AML2 OCI-M1 HEL
c
PIK3C2A Dependency Score (DEMETER2) (Combined RNAi (Broad, Novartis, Marcotte))
NOMO-1
MOLM-13
MV4-11
Mono-Mac-6
THP-1
K-562
LAMA-84
HL-60
Cell lines
DEMETER2
d
HL-60
% Survival
empty vector
PIK3CA OE
PIK3CB OE
PIK3CD OE
PIK3CG OE
Log Conc (M)
HL-60
pRRL-EF1a-PuroR:
3xFLAG (C)-
empty PIK3CA PIK3CB PIK3CD PIK3CG
FLAG
HSP90
130 kDa
100 kDa
100 kDa
e
MV4-11
% Survival
empty vector
PIK3CA OE
PIK3CB OE
PIK3CD OE
PIK3CG OE
Log Conc (M)
MV4-11
pRRL-EF1a-PuroR:
3xFLAG (C)-
empty PIK3CA PIK3CB PIK3CD PIK3CG
FLAG
HSP90
130 kDa
100 kDa
100 kDa

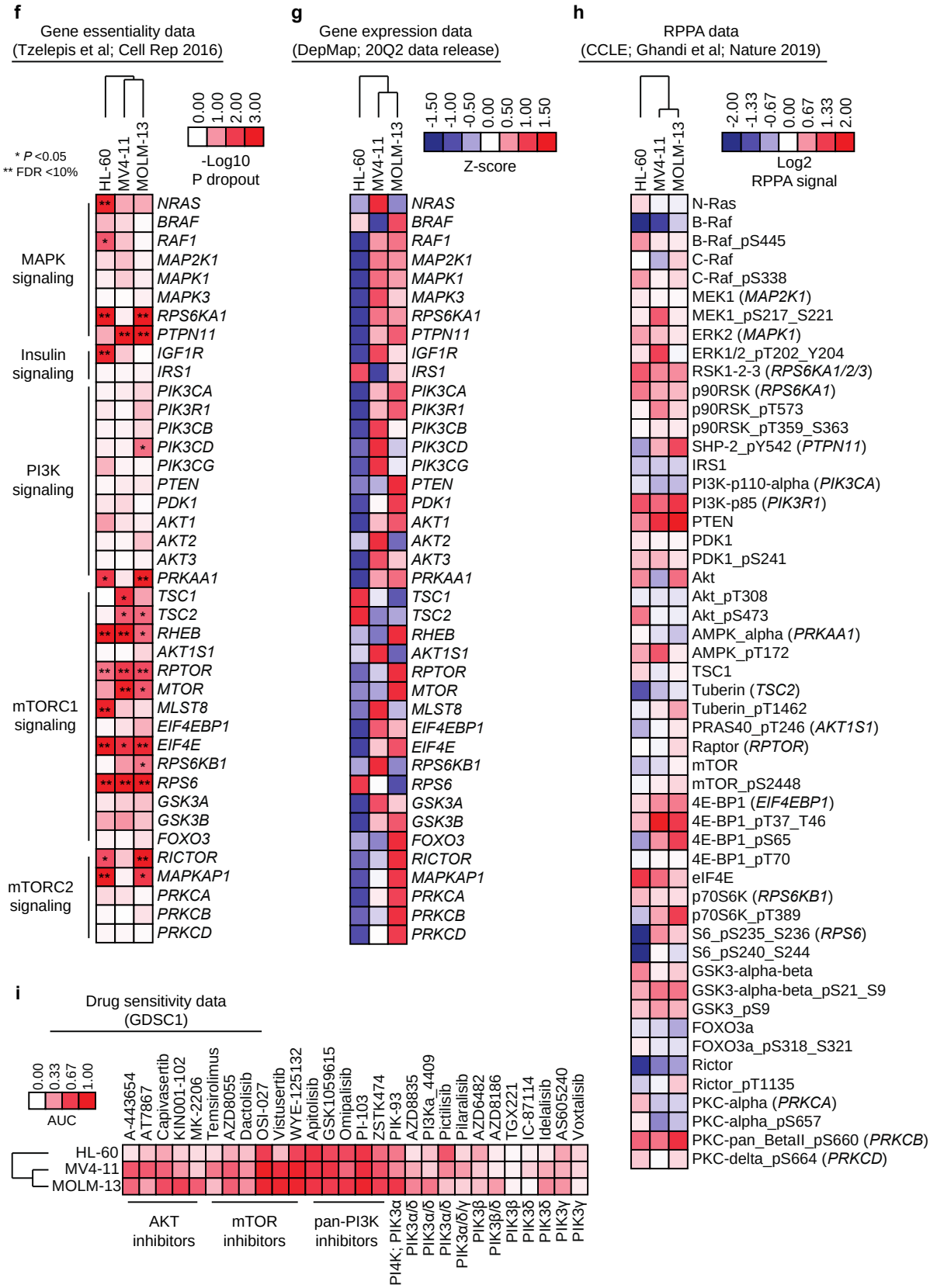

Supplementary Fig. 7| HL-60 cells are vulnerable to PI3K inhibition. a, Distribution of *in vitro* sensitivity (expressed as AUC) to pictilisib among 937 cancer cell lines tested

in the Genomics of Drug Sensitivity in Cancer project (GDSC1)[2]. Data is shown from the top 50 most sensitive lines irrespective of tissue origin or lineage. **b**, Distribution of sensitivity to pictilisib in AML and CML cell lines only. **c**, Cancer cell line genetic dependency to *PIK3C2A* estimated using the DEMETER2 model[3] across 648 cancer cell lines (data retrieved from Cancer Dependency Map portal). The cell lines from this study for which genetic vulnerability data was available are marked. **d**-**e**, Average response to pictilisib in HL-60 and MV4-11 empty vector, and *PIK3CA*, *PIK3CB*, *PIK3CD* or *PIK3CG* overexpressing cells. Error bars indicate standard deviation of the mean of technical triplicates. Data is representative of two independent experiments. Moreover, immunoblot analysis of PIK3CA, PIK3CB, PIK3CD, and PIK3CG expression in HL-60 and MV4-11 cells lentivirally transduced with empty vector, *PIK3CA, PIK3CB, PIK3CD* or *PIK3CG*-cDNA is shown. Data is representative of two independent experiments. **f-l**, Gene essentiality[4], gene expression[5], reverse phase protein array (RPPA)[6], and drug sensitivity data[2], respectively, related to the PI3K/AKT/mTOR signaling in HL-60, MV4-11, and MOLM-13 cells.

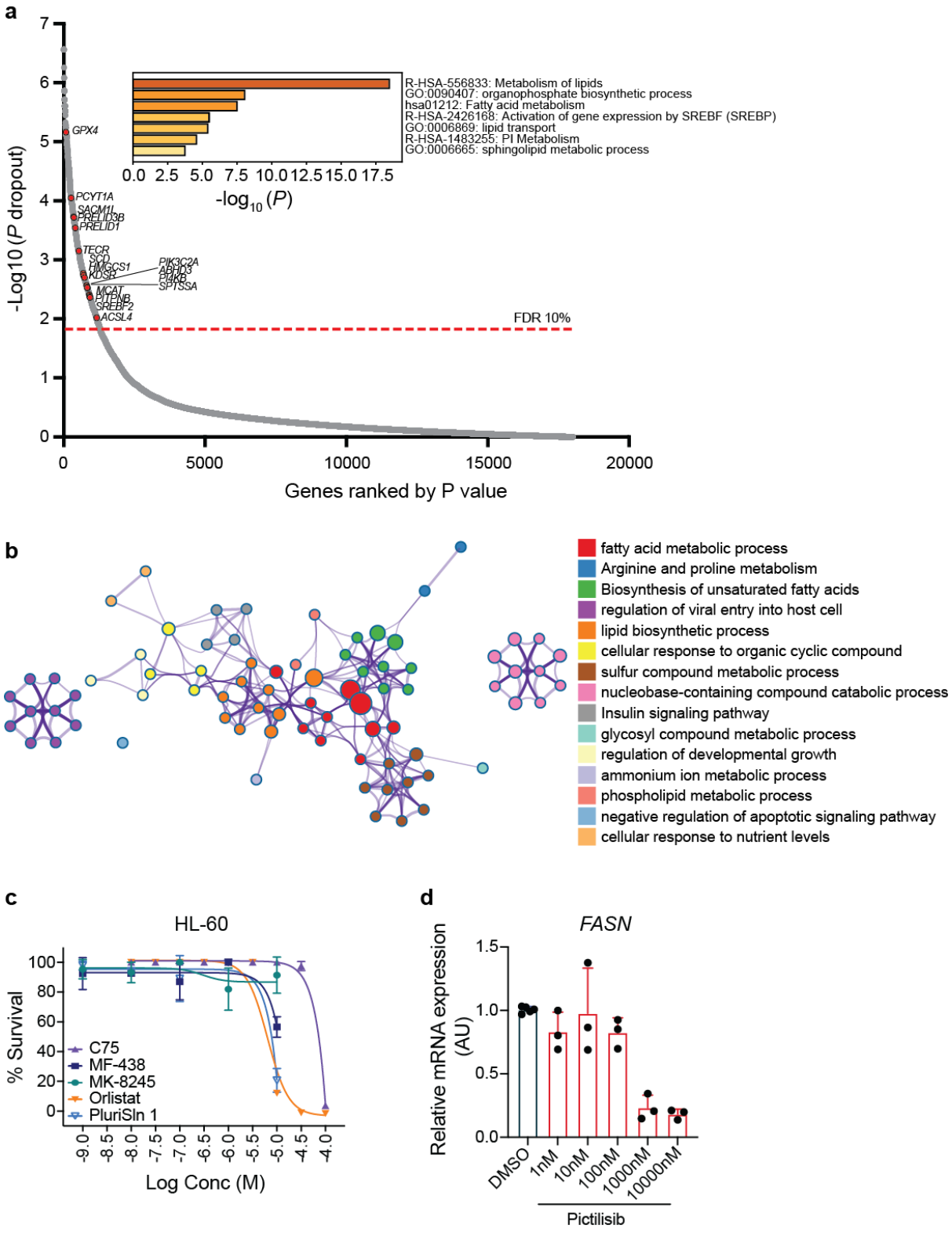

Supplementary Fig. 8| HL-60 cells are dependent on *de novo* FA synthesis. a, Results of genome-wide CRISPR library dropout screen in HL-60 cells. Data obtained from the Yusa lab[4]. Genes involved in lipid metabolism are highlighted in red and gene

enrichment analysis performed with Metascape[7]. **b**, A network layout for enriched ontology clusters of downregulated genes in HL-60 cells generated with Metascape. The network is visualized with Cytoscape (v3.1.2) with “force-directed” layout and with edge bundled for clarity. **c**, Dose response of C75 and orlistat (described to target FASN; technical quadruplicate) as well as 3 stearoyl-CoA desaturase 1 (SCD1; technical duplicate data from original screen) inhibitors in HL-60 cells. Error bars indicate mean ± SD. **d**, *FASN* transcript expression measured by RT-qPCR in response to increasing concentrations of pictilisib treatment. Error bars indicate mean ± SD; (n = 3). Data is representative of two independent experiments

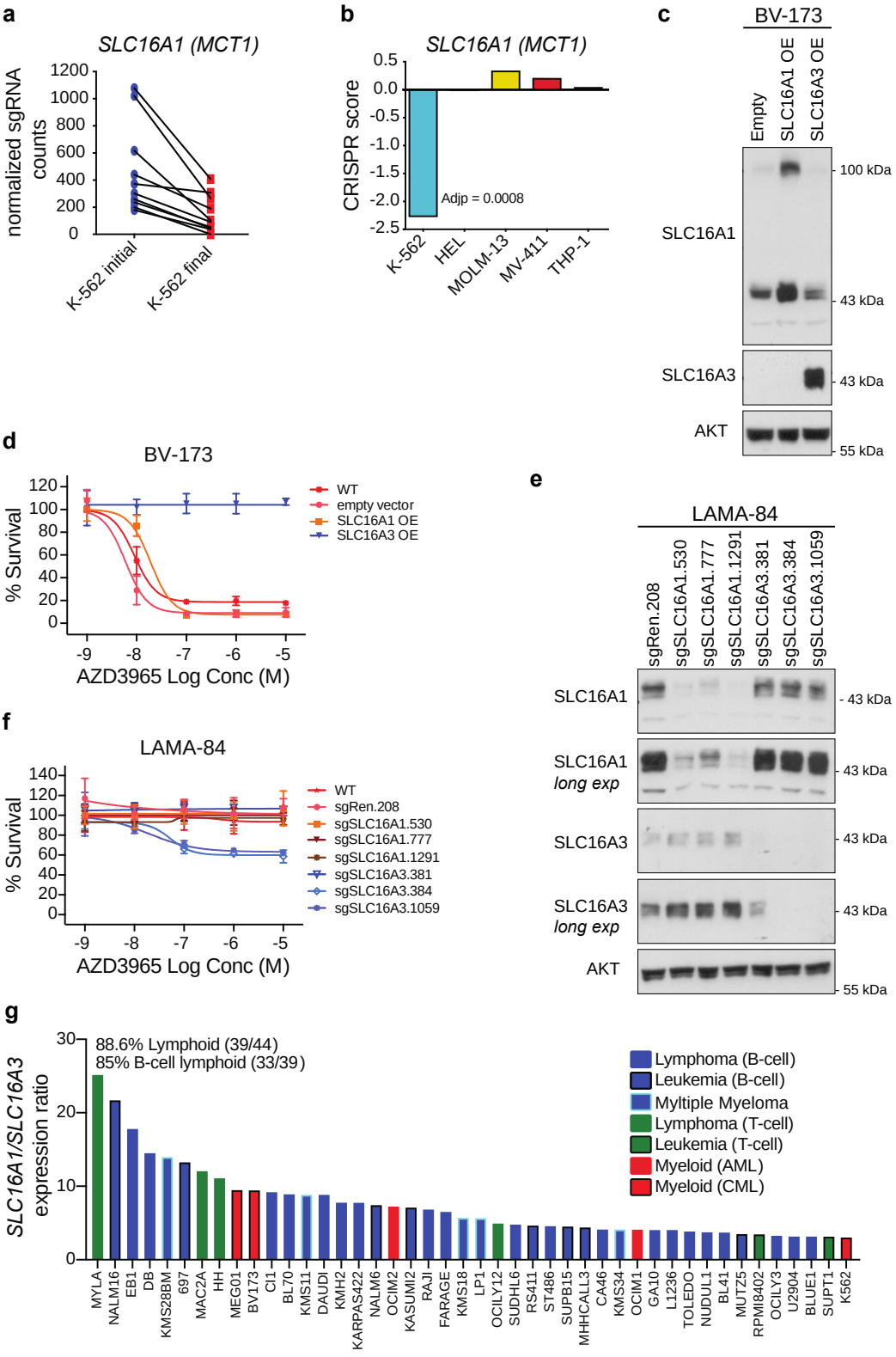

Supplementary Fig. 9| *SLC16A1* essentiality and determinants of sensitivity to the SLC16A1 inhibitor AZD3965. a, Depletion of normalized sgRNA (n = 10) counts for *SLC16A1* in K-562 cells from a CRISPR dropout screen[8], showing that K-562 cells

are dependent on *SLC16A1*. **b**, Comparison of the CRISPR score (a metric to evaluate CRISPR dropout screens and genetic dependencies developed in the Sabatini lab) for the *SLC16A1* in K-562, HEL, MOLM-13, MV4-11, and THP-1 cells. **c**, Immunoblot analysis of SLC16A1 and SLC16A3 expression in BV-173 cells lentivirally transduced with empty vector, *SLC16A1* or *SLC16A3*-cDNA. **d**, Average response to AZD3965 in BV-173 wild type, empty vector, and *SLC16A1* or *SLC16A3* overexpressing cells. **e**, Expression of *SLC16A1* and *SLC16A3* in LAMA-84 CML cells transduced with the indicated sgRNAs. Error bars indicate standard deviation of the mean of technical triplicates. Data is representative of two independent experiments. **f**, Average response to AZD3965 in LAMA-84 wild type, sg*Ren*, and *SLC16A1* or *SLC16A3* deficient cells. Error bars indicate standard deviation of the mean of technical triplicates. Data is representative of two independent experiments. **g**, Distribution of the *SLC16A1*/*SLC16A3* expression ratio across the 44 hematological cancer cell lines predicted to exhibit sensitivity to AZD3965. Bars are colored based on lineage and broad disease subtype. Gene expression data was accessed from the DepMap portal (Expression Public 20Q2)[5].

Supplementary Table 1. Patients' characteristics

Sample ID	Age	Sample type	Diagnosis	Genetics	Status at sampling	Treatment before sampling
Pat.1	> 65	BM	AML with MDS-related changes	No mutations detected	Diagnostic	
Pat.2	< 65	BM	CML, chronic phase	BCR-ABL	Diagnostic	
Pat.3	< 65	PB	CML, blast crisis	BCR-ABL	Refractory disease	dasatinib imatinib nilotinib bosutinib FLAG ponatinib
Pat.4	> 65	PB	AML NOS	*NRAS* G12D	Refractory disease	3+5+7 (daunorubicin, cytarabine, etoposide) followed by mitoxantrone, cytarabine
Pat.5	> 65	PB	sAML post PV	*FLT3*-ITD *JAK2* V617F	Diagnostic	
Pat.6	< 65	PB	AML with mutant NPM1	*NPM1*-B *TP53* polymorphism R72P	Relapse	high dose cytarabine
Pat.7	< 65	BM	CML, blast crisis	BCR-ABL_T315I	Relapse	imatinib nilotinib dasatinib
Pat.8	> 65	BM	AML with mutant NPM1	*NPM1*-A	Diagnostic	
Pat.9	< 65	PB	AML with mutant NPM1	*NPM1*-D *FLT3*-ITD	Relapse	fludarabine cyclophosphamide allogeneic cord blood transplant

Pat.10	> 65	PB	sAML post MPN	*CALR* L367fs*46	Relapse	azacytidine venetoclax
Pat.11	< 65	PB	AML with MDS-related changes	*TP53* R282W heterozygous *TP53* R72P	Relapse	allogenous stem cell transplant cyclophosphamide methotrexate total body irradiation
Pat.12	< 65	PB	AML	N/A	Relapse	azacytidine
Pat.13	> 65	PB	sAML post MDS	DEK-NUP214 *FLT3*-ITD	Relapse	azacytidine hydroxyurea
Pat.14	> 65	PB	AML with MDS-related changes	*IDH1* R132C *RUNX1* F40Wfs*14 *RUNX1* R162K *CBL* C404Y	Relapse	azacytidine
Pat.15	> 65	BM	sAML post MDS/MPN unclassifiable	*ASXL1* Q512* *FLT3*-ITD *PTPN11* S506T *SETBP1* G870S *SRSF2* P95R	Relapse	venetoclax decitabine

MDS-myelodysplastic syndrome; FLAG-fludarabine, arabinofuranosyl cytidine, and granulocyte colony-stimulating factor; NOS-not otherwise specified; sAML-secondary AML; PV-polycythemia vera; MPN-myeloproliferative neoplasm; N/A-not available.

Supplementary References

1 Li, H. *et al.* The landscape of cancer cell line metabolism. *Nat Med* **25**, 850-860, doi:10.1038/s41591-019-0404-8 (2019).

2 Yang, W. *et al.* Genomics of Drug Sensitivity in Cancer (GDSC): a resource for therapeutic biomarker discovery in cancer cells. *Nucleic Acids Res* **41**, D955-961, doi:10.1093/nar/gks1111 (2013).

3 McFarland, J. M. *et al.* Improved estimation of cancer dependencies from large-scale RNAi screens using model-based normalization and data integration. *Nat Commun* **9**, 4610, doi:10.1038/s41467-018-06916-5 (2018).

4 Tzelepis, K. *et al.* A CRISPR Dropout Screen Identifies Genetic Vulnerabilities and Therapeutic Targets in Acute Myeloid Leukemia. *Cell Rep* **17**, 1193-1205, doi:10.1016/j.celrep.2016.09.079 (2016).

5 DepMap, B. DepMap 20Q2 Public. figshare. Dataset. https://doi.org/10.6084/m9.figshare.12280541.v4. (2020).

6 Ghandi, M. *et al.* Next-generation characterization of the Cancer Cell Line Encyclopedia. *Nature* **569**, 503-508, doi:10.1038/s41586-019-1186-3 (2019).

7 Zhou, Y. *et al.* Metascape provides a biologist-oriented resource for the analysis of systems-level datasets. *Nat Commun* **10**, 1523, doi:10.1038/s41467-019-09234-6 (2019).

8 Wang, T. *et al.* Identification and characterization of essential genes in the human genome. *Science* **350**, 1096-1101, doi:10.1126/science.aac7041 (2015).